A Relative Infrastructure-less Localization Algorithm for Decentralized and Autonomous Swarm Formation

Dominik Schindler, Vlad Niculescu, Tommaso Polonelli, Daniele Palossi, Luca Benini, and Michele Magno

***Abstract*— Decentralized and autonomous control of Unmanned Aerial Vehicle (UAV) swarms is a key enabler for cooperative systems and infrastructure-less formation flights. However, UAVs often lack reliable heading angle measurements, especially in indoor scenarios, space, and GNSS-denied environments, posing an additional observability challenge on range-based relative localization. We tackle this problem by proposing a novel solution enhancing the classical tag-and-anchor trilateration. The proposed solution relies on Ultra-wideband range measurements and addresses the relative pose estimation between pairs of UAVs under relative motion. Furthermore, it does not require any explicit motion pattern or initialization procedure and leverages an approximate maximum-likelihood algorithm to recursively solve the relative localization problem with constant computational complexity. The method has been implemented and demonstrated through field experiments, where a swarm of nano-UAVs positioned themselves with respect to a leader in a *nearly*-static formation with an average error of $38.5\,\mathrm{cm}$ and a convergence time of $25\,\mathrm{s}$. The achieved formation accuracy is similar to the one achieved by the state-of-the-art EKF-based leader-follower methods.**

I. Introduction

The collaboration of a swarm of robots can enhance the capabilities of individual agents by harnessing collective advantages. This cooperative approach aims to minimize latency, enhance robustness, and increase adaptability, unlocking new opportunities for achieving shared objectives [1]. Several tasks can be carried out effectively and at low latency by a swarm of robots [2], such as cooperative mapping and localization, object detection, and explorations. Agents joining a cooperating swarm must remain operable in a group [3], perceiving and communicating with neighbors preferably without relying on external infrastructure [4], [5]. Apart from common features like obstacle avoidance and environmental perception [6], a swarm agent needs to measure its relative location among other agents to handle the formation and infer the optimal mission strategy based on the neighbor's position. Although the relative and absolute location estimation of neighbors in a swarm is a solved mathematical problem, existing methods often do not satisfy today's practical deployment requirements, lacking robustness under non-ideal conditions such as high sensor measurement noise [3], [5].

All authors are with the Department of Information Technology and Electrical Engineering (D-ITET), ETH Zürich, Switzerland

D. Palossi is also with Dalle Molle Institute for Artificial Intelligence (IDSIA), USI-SUPSI, Switzerland

L. Benini is also with the Department of Electrical, Electronic and Information Engineering (DEI), University of Bologna, Italy

V. Niculescu is the corresponding author: vladn@ethz.ch

A popular and lightweight solution for absolute and relative localization is based on Ultra-Wideband (UWB) radio transceivers because of their relatively high accuracy in the decimeter range without the support of external references or infrastructure. UWB is particularly beneficial in several challenging application scenarios [7], such as in Global Navigation Satellite System (GNSS) denied environments, space, and indoor navigation, where sensing limitations could make the relative UAV position estimation unobservable [7], [8]. One of the most common sensing limitations regards the navigation heading: magnetometers, the most common solution for measuring the absolute heading, heavily suffer from magnetic distortions, e.g., due to ferromagnetic building construction materials and electric motor currents [3], [5].

This work proposes an approach to enable the infrastructure-less formation of a swarm of robots relying on onboard inertial and odometry measurements, point-to-point distance measurements among pairs of agents (based on UWB), and wireless local data exchange. This work leads to the development and field demonstration of a relative localization algorithm that is independent of direct heading measurements. The proposed solution is able to operate with small relative motion solely originating from feedback control fluctuations, enabling a near-static formation, not requiring any explicit motion pattern or initialization. Collected results on Nano Unmanned Aerial Vehicles (UAVs), characterized by limited computational and sensing capabilities, show a mean formation error of $38.5\,\mathrm{cm}$ and a convergence time of $25\,\mathrm{s}$ even in the presence of noisy measurements.

In detail, the contributions of this paper are: *(i)* A novel Relative Pose Estimation Method: The novel method presented in this paper improves over existing EKF-based methods [3], [5], [12] as it does not require initial calibrations. Furthermore, the method finds a global optimum, and it is robust to divergence. Moreover, a recursive formulation enables the incorporation of an arbitrary number of exponentially-weighted measurements over time at a maximum rate of $250\,\mathrm{Hz}$. *(ii)* Optimized Trilateration Algorithm: A key enabler for this work is a new trilateration algorithm that solves an approximate maximum-likelihood trilateration problem. We found that our method improves over the popular *differences of squares* (DoS) [14] by eliminating its typical large errors in short baseline scenarios [8], [15]. *(iii)* Static Formation Flight: Based on the relative pose estimation method, a decentralized formation controller is developed and demonstrated with practical experiments. The formation showcases the robustness of the relative pose estimation method. With a near-static formation, the swarm

TABLE I: Overview of formation flight and relative pose estimation methods.

Method	Measurements Bearing / Heading	Required motion	Initialization	Experiment
Nägeli *et al.* [9]	Yes / Yes	None	Not reported	3 UAVs static formation (no leader)
Zhou *et al.* [10]	No / No	Random	Five initial measurements	UGV relative pose estimation
Wang *et al.* [11]	No / Yes	Manual control	None	UAV relative pose estimation
Guo *et al.* [12]	No / Yes	Piece-wise linear	EKF initial measurements	3 UAVs relative motion
Coppola *et al.* [3]	No / Yes	Collision avoidance	EKF initial values predefined	3 UAVs collision avoidance
Helm *et al.* [5]	No / No	Trajectory	EKF initial values predefined	UAV leader-follower (time offset)
Li *et al.* [4]	No / No	Trajectory	EKF initial values determined	5 UAVs leader-follower
Güler *et al.* [13]	Yes / No	Sinusoidal leader	None	2 UAVs static formation (with leader)
Our work	**No / No**	**None (static leader)**	**None**	**5 UAVs static formation (with leader)**

was able to operate on the boundary of observability since all relative motion between the robots originates from sensor and actuator noise as well as the resulting estimation and control inaccuracies. We provide code and further details on our algorithms on GitHub [1].

II. Related work

Decentralized relative localization is a well-known problem in robotics swarm operations, from ground vehicles [10] to aerial multi-copters [3], [5], [9], [11]–[13], [16]. Many different techniques have been proposed over time, employing various types of sensors, from GPS [16] to vision-based approaches [9] and radio ranging solutions [3], [5], [11]–[13]. Addressing this problem with GPS limits its applicability to outdoor applications, like in [16], where the authors addressed the problem of static formation control on drone swarms. Vision-based algorithms represent an appealing alternative, such as [9], where the authors addressed the problem of relative position estimation. Although, camera-based systems suffer from image processing computational requirements (not always met by processors aboard the robot), limited field of view, and occlusions.

In contrast, our work focuses on radio ranging which typically employs omnidirectional radio sources such as Bluetooth [3] or UWB [4], [5], [12], [13]. In the latter case, Angle of Arrival (AoA) methods can provide directional information from the phase differences of multiple antennas [17], angle-dependent variations of the channel impulse response [18], or by using multiple UWB transmitters [13]. When AoA is not employed [5], [11], [12], directional information can be retrieved by communicating state information computed locally, e.g., the odometry of the robot, or by estimating relative localization from range measurements and the relative motion between nodes. In these cases, the system's observability plays a crucial role. Results from [10] show how ground vehicle observability in 2D relative localization is possible only if the relative motion is constrained. Similarly, in [4], [5], the authors show how the lack of a common heading reference (e.g., the north of a magnetometer) strongly impacts the achievable accuracy.

Various methods have been proposed for ranging-based relative localization of UAVs without directional information, such as particle filter variations [13], moving horizon estimation with convex optimization [11], and EKF-based approaches [3], [5], [12]. This last group is a compelling alternative due to its low computational and memory requirements compared to moving horizon methods [11], which suffer from high computational costs for large moving horizon windows. Authors in [5] propose a solution for the relative localization of UAVs without common heading reference. The authors designed an EKF-based relative localization algorithm and integrated it into a leader-follower swarm control system. Their results are particularly interesting for indoor UAVs where magnetometer measurements are not reliable or available, such as in [3], where the heading is estimated using gyroscope integration only.

However, EKF-based approaches need good initial values to converge, which is not available for many practical applications [4], [5], [12]. Therefore, this work presents a novel method that improves over existing EKF-based solutions [3], [5], [12] by not requiring any initial values and heading measurements. Our method finds the global optimum, showing robustness to divergence and inconsistency, similar to the moving horizon estimation [11]. Finally, a recursive formulation enables the incorporation of an arbitrary number of exponentially-weighted measurements over time. In Table I, we report an exhaustive comparison of the formation flight and the pose estimation methods of the aforementioned works w.r.t. the proposed one.

III. Algorithms

A. An Approximative Maximum-Likelihood Trilateration

Trilateration is a method to determine the position of a static or mobile object given its distance from a set of stationary locations with known positions (i.e., anchors). Due to its good trade-off between accuracy and computational demands, trilateration was used in many localization applications [8], [15]. The mathematical formulation of the trilateration is expressed with the following notation: $\{d_k\}_{k=1}^{n}$ are the distances from each of the n anchors with known coordinates $\left\{\boldsymbol{p}_{\text{ANCHOR},k}\right\}_{k=1}^{n}$ as shown in Figure 1. If noise-free range measurements are assumed, then finding the UAV's position comes down to finding intersections of circles (2D) or spheres (3D), requiring at least 3 or 4 anchors, respectively [8]. However, in real-world applications, range

[1] https://github.com/ETH-PBL/swarm-relative-localization

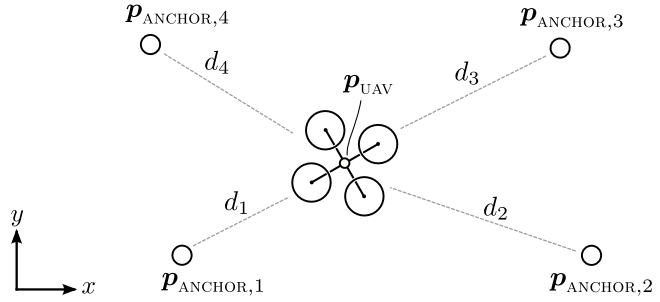

Fig. 1: In the classical trilateration problem, the position of a UAV is computed based on range measurements $\{d_1, \dots, d_n\}$ to n anchors of known locations.

measurements are affected by noise, and therefore the classical geometrical methods lead to a poor localization accuracy [8]. Under the assumption of zero-mean Gaussian noise on the range measurements, the maximum-likelihood (ML) estimate of the UAV's position $\boldsymbol{p}_{\text{UAV}}$ is found by minimizing the sum of the squared ranging error residuals [15], as shown in Equation 1. We note as w_k the noise corrupting the range measurements.

$$\boldsymbol{p}_{\text{UAV}}^{\text{ML}} = \underset{\boldsymbol{p}_{\text{UAV}}}{\arg\min} \sum_{i=1}^{n} \left(\underbrace{\left\| \boldsymbol{p}_{\text{UAV}} - \boldsymbol{p}_{\text{ANCHOR},i} \right\| - d_i}_{w_i} \right)^2 \tag{1}$$

In the following, we propose an algorithm that tackles the optimization problem of Equation 1 and then we show how it can be further extended to address the UAV relative localization problem in real-world scenarios. Thus, the optimization problem is rewritten from Equation 1 by introducing an equality constraint for w_i, as shown in Equation 2.

$$\begin{aligned} \boldsymbol{p}_{\text{UAV}}^{\text{ML}} &= \underset{\boldsymbol{p}_{\text{UAV}}}{\arg\min} \sum_{i=1}^{n} w_i^2 \\ \text{s.t.} \quad & w_i = d_i - \left\| \boldsymbol{p}_{\text{UAV}} - \boldsymbol{p}_i \right\| \end{aligned} \tag{2}$$

In order to derive an approximation to the ML cost function, we consider the unit length vectors $\{\boldsymbol{e}_i\}_{i=1}^n$ in the range measurement directions,

$$\boldsymbol{e}_i (d_i - w_i) = \boldsymbol{p}_{\text{UAV}} - \boldsymbol{p}_i \tag{3}$$

Consequently, for two anchors i and j holds

$$\boldsymbol{e}_j (d_j - w_j) = \boldsymbol{e}_i (d_i - w_i) + \boldsymbol{p}_i - \boldsymbol{p}_j \tag{4}$$

Taking the squared norm on both sides, it expands to

$$\begin{aligned} d_j^2 - 2\, d_j w_j + w_j^2 = d_i^2 - 2\, d_i w_i + w_i^2 \\ + 2\,(d_i - w_i)\, \boldsymbol{e}_i^{\mathsf{T}} \left(\boldsymbol{p}_i - \boldsymbol{p}_j \right) + \left\| \boldsymbol{p}_i - \boldsymbol{p}_j \right\|^2 \end{aligned} \tag{5}$$

Assuming $|w_i| \ll |d_i|$, the approximation $-2\, d_i w_i + w_i^2 \approx -2\, d_i w_i$ holds. Applying this approximation for i and j and defining

$$\boldsymbol{d}_i := (d_i - w_i)\, \boldsymbol{e}_i = \boldsymbol{p}_{\text{UAV}} - \boldsymbol{p}_i \tag{6}$$

yields

$$w_j = \boldsymbol{d}_i^{\mathsf{T}} \frac{\left(\boldsymbol{p}_j - \boldsymbol{p}_i \right)}{d_j} + w_i \frac{d_i}{d_j} - \frac{\left\| \boldsymbol{p}_j - \boldsymbol{p}_i \right\|^2 + d_i^2 - d_j^2}{2\, d_j} \tag{7}$$

We approximate the objective function of Equation 2 with the approximation from Equation 7 and note that the resulting objective is a function of w_i and $\boldsymbol{d}_i$ only where i is the index of an arbitrarily chosen anchor. The constraint of Equation 2 for w_j and $j \neq i$ are trivial to satisfy because the objective function of the approximate problem does not depend on w_j. Therefore, the corresponding constraints are dropped. We state the approximation to Equation 2 explicitly as

$$\boldsymbol{p}_{\text{UAV}}^{\text{ML}} \approx \boldsymbol{p}_i + \boldsymbol{d}_i^* \tag{8}$$

and $\boldsymbol{d}_i^*$ being the solution to the approximate ML optimization problem

$$\begin{aligned} \boldsymbol{d}_i^*, w_i^* &= \underset{\boldsymbol{d}_i, w_i}{\arg\min}\, f(\boldsymbol{d}_i, w_i) \\ \text{s.t.} \quad & g(\boldsymbol{d}_i, w_i) = \left\| \boldsymbol{d}_i \right\|^2 - (d_i - w_i)^2 = 0 \end{aligned} \tag{9}$$

with the *single* quadratic equality constraint $g(\boldsymbol{d}_i, w_i)$ and the quadratic objective function $f(\boldsymbol{d}_i, w_i)$.

$$\begin{aligned} f(\boldsymbol{d}_i, w_i) = \sum_{j=1}^{n} \Bigg(& \boldsymbol{d}_i^{\mathsf{T}} \frac{\left(\boldsymbol{p}_j - \boldsymbol{p}_i \right)}{d_j} \\ & + w_i \frac{d_i}{d_j} - \frac{\left\| \boldsymbol{p}_j - \boldsymbol{p}_i \right\|^2 + d_i^2 - d_j^2}{2\, d_j} \Bigg)^2 \end{aligned} \tag{10}$$

To make a step forward towards solving the quadratic problem in Equation 9, we rewrite it in matrix form.

$$\begin{aligned} f(\boldsymbol{d}_i, w_i) = & \begin{pmatrix} \boldsymbol{d}_i \\ w_i \end{pmatrix}^{\mathsf{T}} \underbrace{\left(\sum_{j=1}^{n} \boldsymbol{Q}_j \right)}_{\boldsymbol{Q}} \begin{pmatrix} \boldsymbol{d}_i \\ w_i \end{pmatrix} \\ & - 2 \underbrace{\left(\sum_{j=1}^{n} \boldsymbol{c}_j^{\mathsf{T}} \right)}_{\boldsymbol{c}} \begin{pmatrix} \boldsymbol{d}_i \\ w_i \end{pmatrix} + \underbrace{\left(\sum_{j=1}^{n} e_j \right)}_{e} \end{aligned} \tag{11}$$

with the following coefficients.

$$\boldsymbol{Q}_j = \begin{pmatrix} \frac{1}{d_j^2} \left(\boldsymbol{p}_j - \boldsymbol{p}_i \right) \left(\boldsymbol{p}_j - \boldsymbol{p}_i \right)^{\mathsf{T}} & \frac{d_i}{d_j^2} \left(\boldsymbol{p}_j - \boldsymbol{p}_i \right) \\ \frac{d_i}{d_j^2} \left(\boldsymbol{p}_j - \boldsymbol{p}_i \right)^{\mathsf{T}} & \frac{d_i^2}{d_j^2} \end{pmatrix} \tag{12}$$

$$\boldsymbol{c}_j = \frac{\left\| \boldsymbol{p}_j - \boldsymbol{p}_i \right\|^2 + d_i^2 - d_j^2}{2\, d_j^2} \begin{pmatrix} \boldsymbol{p}_j - \boldsymbol{p}_i \\ d_i \end{pmatrix} \tag{13}$$

$$e_j = \left(\frac{\left\| \boldsymbol{p}_j - \boldsymbol{p}_i \right\|^2 + d_i^2 - d_j^2}{2\, d_j} \right)^2 \tag{14}$$

In previous formulations, we show how the trilateration problem is reduced to solving the constrained optimization problem with the quadratic objective function $f(\boldsymbol{d}_i, w_i)$ given by Equation 10 and the equality constraint $g(\boldsymbol{d}_i, w_i)$ given in Problem 9. In the following, we show how to solve this problem, and considering the case of a 3D Euclidean space, we note $\boldsymbol{d}_i = (x, y, z)^{\mathsf{T}}$. From the *method of Lagrange*

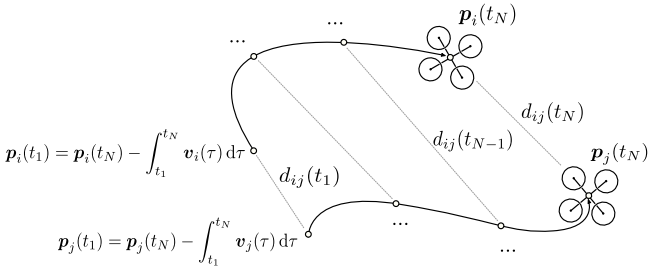

Fig. 2: The range-based relative localization problem.

multipliers, Equations 15 – 16 must hold for the solution to the minimization problem.

$$0 = \frac{1}{2}\left(\nabla f(\boldsymbol{d}_i, w_i) - \lambda \nabla g(\boldsymbol{d}_i, w_i)\right) = \boldsymbol{Q}_\lambda \begin{pmatrix} \boldsymbol{d}_i \\ w_i \end{pmatrix} - \boldsymbol{c}_\lambda \tag{15}$$

$$0 = g(\boldsymbol{d}_i, w_i) = x^2 + y^2 + z^2 - w_i^2 + 2\,d_i w_i - d_i^2 \tag{16}$$

The matrix $\boldsymbol{Q}_\lambda$ and the vector $\boldsymbol{c}_\lambda$ are defined for simplicity of the mathematical treatment and defined by Equations 17 – 18. The conditions are a non-linear equation system with the five unknowns x, y, z, w_i, and λ.

$$\boldsymbol{Q}_\lambda := \boldsymbol{Q} + \begin{pmatrix} -\lambda & 0 & 0 & 0 \\ 0 & -\lambda & 0 & 0 \\ 0 & 0 & -\lambda & 0 \\ 0 & 0 & 0 & \lambda \end{pmatrix} \tag{17}$$

$$\boldsymbol{c}_\lambda := \boldsymbol{c} + \begin{pmatrix} 0 & 0 & 0 & d_i\lambda \end{pmatrix}^\mathsf{T} \tag{18}$$

In a first step, the sub-system $\boldsymbol{Q}_\lambda \begin{pmatrix} \boldsymbol{d}_i^\mathsf{T} & w_i \end{pmatrix}^\mathsf{T} = \boldsymbol{c}_\lambda$ is solved with *Cramer's rule*. We note as $\mathrm{DET}_x(\lambda)$, $\mathrm{DET}_y(\lambda)$, $\mathrm{DET}_z(\lambda)$, and $\mathrm{DET}_{w_i}(\lambda)$ the determinants of the matrices obtained by replacing the first, second, third and fourth column of $\boldsymbol{Q}_\lambda$ with $\boldsymbol{c}_\lambda$, respectively. From Cramer's rule, the solution (i.e., x, y, z and w_i) is obtained by dividing each of the introduced determinants by $\mathrm{DET}_{\boldsymbol{Q}_\lambda}(\lambda)$. All determinants are polynomials in λ of degree ≤ 4, and therefore each solution depends on λ. Inserting the solution from Cramer's rule into Equation 16 yields a polynomial of degree eight as shown in Equation 19. The real roots of the resulting polynomials are candidates for the optimal Lagrange multiplier. With back-substitution into Cramer's solutions, a candidate for the complete solution is found. Finally, the optimal solution is found by checking the objective function with each candidate. Polynomial roots can be computed efficiently with a numerical Eigenvalue solver.

$$\begin{aligned} &\mathrm{DET}_x(\lambda)^2 + \mathrm{DET}_y(\lambda)^2 + \mathrm{DET}_z(\lambda)^2 - \mathrm{DET}_{w_i}(\lambda)^2 + \\ &2\,d_i\,\mathrm{DET}_{w_i}(\lambda)\,\mathrm{DET}_{\boldsymbol{Q}_\lambda}(\lambda) - d_i^2\,\mathrm{DET}_{\boldsymbol{Q}_\lambda}(\lambda)^2 = 0 \end{aligned} \tag{19}$$

B. Range-based Relative Pose Estimation of UAVs

Section III-A presented a solution for determining the position of a UAV, by knowing the distances to known-position anchors. In this section, we consider an adapted scenario that only considers two moving UAVs (i.e., no anchor) and attempts to find their relative position and heading (i.e., pose). The two UAVs, i and j, are assumed to be moving simultaneously with velocities $\boldsymbol{v}_i(t)$ and $\boldsymbol{v}_j(t)$ such that they obtain the positions $\boldsymbol{p}_i(t)$ and $\boldsymbol{p}_j(t)$. At discrete time steps t_k, $k \in \{1, \ldots, N\}$, range measurements $d_{ij}(t_k)$ are taken between drone i and j. We assume that each drone can estimate its own velocity from its onboard state estimator. Furthermore, we assume that drone i continuously receives the velocity and distance measurements from drone j and vice-versa. Figure 2 shows an illustration of the scenario. From the elementary laws of motion, the equation $\boldsymbol{p}_i(t_k) = \boldsymbol{p}_i(t_N) - \int_{t_k}^{t_N} \boldsymbol{v}_i(\tau)\,\mathrm{d}\tau$ holds. Writing this equation for two drones and computing the difference allows formulating the ML estimation problem that is given in Equation 20, where $\boldsymbol{d}_{ij}(t) = \boldsymbol{p}_j(t) - \boldsymbol{p}_i(t)$ is the relative position of the two. We highlight the similarity of Equation 2 with Equation 20, where the relative position $\boldsymbol{d}_{ij}(t)$ takes the role of UAV's position, and the integral takes the role of the anchor's position. This similarity is important because we can use the same method described in Section III-A to solve the optimization problem in Equation 20. However, note that while Equation 2 sums over all anchors i, in Equation 20, the sum is performed over all discrete time steps of a relative localization scenario defined by the timestamps k, while i and j are fixed because the relative position is determined for two drones at a time.

$$\begin{aligned} &\boldsymbol{d}_{ij}^{\mathrm{ML}}(t_N) = \underset{\boldsymbol{d}_{ij}(t_N)}{\arg\min} \sum_{k=1}^{N} w_k^2 \\ &\text{s.t.} \quad w_k = \|\boldsymbol{d}_{ij}(t_N) - \int_{t_k}^{t_N} \boldsymbol{v}_j(\tau) - \boldsymbol{v}_i(\tau)\,\mathrm{d}\tau\| - d_{ij}(t_k) \end{aligned} \tag{20}$$

The scenario described so far assumes both drone i and j are aligned within the same gravity-aligned coordinate frame, and so are the velocity measurements $\boldsymbol{v}_i$ and $\boldsymbol{v}_j$. However, in the real world, the UAVs do not have any means of performing absolute heading measurements, and the heading is only estimated by integrating the angular velocity over time (typically provided by gyroscopes). Therefore, factors such as different heading angles at take-off or gyroscope drift can result in a significant misalignment between the coordinate frames of the drones. To account for this, we note as L_i and L_j the gravity-aligned coordinate frames of drones i and j, respectively, and introduce the transformation matrix between the two coordinate frames $\boldsymbol{T}_{L_iL_j}(t)$, defined by the z-axis rotation matrix for the angle ψ_{ij}. $\psi_{ij}(t)$ is the relative heading angle, and $\dot{\psi}_{ij}(t)$ is its rate of change, which is unknown but very small.

Each UAV $i \in \{1, \ldots, n\}$ is capable of onboard velocity measurements ${}_{L_i}\boldsymbol{v}_i(t)$ in its local coordinate frame. This velocity allows obtaining the local position displacement from time t_k to t_N, which we note as $\boldsymbol{\rho}_{i,k} := \int_{t_k}^{t_N} {}_{L_i}\boldsymbol{v}_i(\tau)\,\mathrm{d}\tau$ to simplify the notation. In the following, we rewrite Equation 20 so that it accounts for the different coordinate frames and the relative rotation between those. The final form of the pair-wise pose estimation problem is given in Equation 21. In the formula, $\boldsymbol{T}_{L_iL_j}$ is assumed constant although is exhibits yaw drift in reality. The odometry constraints given by $\boldsymbol{\rho}_{i,k}$, $\boldsymbol{\rho}_{j,k}$ also exhibit drift. To accommodate these two effects,

the formula has an exponentially decaying weighting of old measurements with a time constant τ.

$$ {}_{L_i}\hat{\boldsymbol{d}}_{ij,N}, \hat{\boldsymbol{T}}_{L_iL_j,N} = \arg\min \sum_{k=1}^{N} \mathrm{e}^{-\frac{t_N - t_k}{\tau}} w_k^2 \tag{21} $$
$$ \text{s.t.} \quad w_k = \left\| {}_{L_i}\boldsymbol{d}_{ij,N} + \boldsymbol{\rho}_{i,k} - \boldsymbol{T}_{L_iL_j} \boldsymbol{\rho}_{j,k} \right\| - d_{ij,k} $$

C. Recursive Solution for the Relative Pose Estimation

In the following, we propose a solution to solve the complete relative localization problem given in Equation 21. Since the goal is to determine both relative position and heading, we refer to this as the relative pose estimation, which is the ultimate goal of this work. Therefore, we propose solving the optimization problem in Equation 21 by firstly solving for $\boldsymbol{d}_{ij,N}$ and then for ψ_{ij} as shown in Equation 22. We propose solving the outer optimization problem by performing an exhaustive search over the full range of possible relative heading angles.

$$ \min_{\psi_{ij} \in \{0^\circ, \dots, 359^\circ\}} \left(\min_{{}_{L_i}\boldsymbol{d}_{ij,N}} \sum_{k=1}^{N} \mathrm{e}^{-\frac{t_N - t_k}{\tau}} w_k^2 \right) \tag{22} $$

Next, we solve the inner optimization problem by relying on the approach from Section III-A. We provide an equivalent formulation to Problem 21 where the odometry constraint is formulated recursively and note $\boldsymbol{T}_{L_iL_j}$ as $\boldsymbol{T}(\psi_{ij})$.

$$ {}_{L_i}\hat{\boldsymbol{d}}_{ij,k}(\psi_{ij}),\ \hat{w}_{ij,k}(\psi_{ij}) = \underset{{}_{L_i}\boldsymbol{d}_{ij,k}, w_{ij,k}}{\arg\min} \sum_{k=1}^{N} \mathrm{e}^{-\frac{t_{k+1} - t_k}{\tau}} w_k^2 \tag{23} $$
$$ \text{s.t.} \ \ w_k = \| {}_{L_i}\boldsymbol{d}_{ij,k} \| - d_{ij,k} $$
$$ {}_{L_i}\boldsymbol{d}_{ij,k+1} = {}_{L_i}\boldsymbol{d}_{ij,k} + \int_{t_k}^{t_{k+1}} \boldsymbol{T}(\psi_{ij})\, {}_{L_j}\boldsymbol{v}_j(\tau) - {}_{L_i}\boldsymbol{v}_i(\tau)\, \mathrm{d}\tau $$

Approximating the odometry constraint (i.e., the second one) with the *Euler forward* integration of the relative position ${}_{L_i}\boldsymbol{d}_{ij}$ leads to Equation 24. We note $\Delta t = t_{k+1} - t_k$.

$$ {}_{L_i}\boldsymbol{d}_{ij,k+1} = {}_{L_i}\boldsymbol{d}_{ij,k} - \underbrace{\left({}_{L_i}\boldsymbol{v}_{i,k} - \boldsymbol{T}(\psi_{ij})\, {}_{L_j}\boldsymbol{v}_{j,k} \right) \Delta t}_{\boldsymbol{u}_k(\psi_{ij})} \tag{24} $$

For a recursive formulation of Problem 23, we denote the objective function of the time step k as $f_k(\boldsymbol{d}_{ij,k}, w_{ij,k}, \psi_{ij})$. For time step $k+1$ a new range measurement $d_{ij,k}$ is considered, augmenting the optimization problem to Equation 25.

$$ \min \quad f_k(\boldsymbol{d}_{ij,k}, w_{ij,k}, \psi_{ij})\, \mathrm{e}^{-\frac{t_{k+1} - t_k}{\tau}} + w_{ij,k+1}^2 \tag{25} $$
$$ \text{s.t.} \quad \|\boldsymbol{d}_{ij,k}\|^2 = (d_{ij,k} - w_{ij,k})^2 $$
$$ \|\boldsymbol{d}_{ij,k+1}\|^2 = (d_{ij,k+1} - w_{ij,k+1})^2 $$

In order to make the recursion in Problem 25 mathematically tractable, the same approximation and matrix formulation as in the trilateration case are applied. With the affine approximation from Equation 7, we derive

$$ w_{ij,k} = \frac{\boldsymbol{u}_k(\psi_{ij})^\mathsf{T}}{d_{ij,k}} {}_{L_i}\boldsymbol{d}_{ij,k+1} + \frac{d_{ij,k+1}}{d_{ij,k}} w_{ij,k+1} - \frac{\|\boldsymbol{u}_k(\psi_{ij})\|^2 + d_{ij,k+1}^2 - d_{ij,k}^2}{2\, d_{ij,k}} \tag{26} $$

We substitute $w_{ij,k}$ from Equation 26 and ${}_{L_i}\boldsymbol{d}_{ij,k}$ from Equation 24 into the recursive objective function from Equation 25. Consequently, we obtain an objective function of the same form as Equation 11, with the mention that $\boldsymbol{Q}$, $\boldsymbol{c}$ and e now depend on the time index k and angle ψ_{ij}. We mention that the first constraint of Equation 25 is independently satisfied by the objective function and therefore can be discarded. In conclusion, we showed how the relative localization is reduced to the same mathematical problem as the trilateration and therefore solved using the solution given in Section III-A. However, in this case the matrices $\boldsymbol{Q}$, $\boldsymbol{c}$ and e have different values, and we give then in Equations 27 – 31. To simplify the notation, we omitted the dependency on the angle ψ_{ij}.

$$ \boldsymbol{Q}_{k+1} = \begin{pmatrix} \boldsymbol{0} & \boldsymbol{0} \\ \boldsymbol{0}^\mathsf{T} & 1 \end{pmatrix} + \mathrm{e}^{-\frac{t_{k+1} - t_k}{\tau}} \left(\boldsymbol{A}_k^\mathsf{T}\, \boldsymbol{Q}_k\, \boldsymbol{A}_k \right) \tag{27} $$
$$ \boldsymbol{c}_{k+1}^\mathsf{T} = \mathrm{e}^{-\frac{t_{k+1} - t_k}{\tau}} \left(\boldsymbol{c}_k^\mathsf{T} \boldsymbol{A}_k + \boldsymbol{b}_k^\mathsf{T} \boldsymbol{Q}_k\, \boldsymbol{A}_k \right) \tag{28} $$
$$ e_{k+1} = \mathrm{e}^{-\frac{t_{k+1} - t_k}{\tau}} \left(e_k + \boldsymbol{b}_k^\mathsf{T} \boldsymbol{b}_k \right) \tag{29} $$

where $\boldsymbol{A}_k$ and $\boldsymbol{b}_k$ are the linear transformation from Equations 24 and 26 in matrix form.

$$ \boldsymbol{A}_k = \begin{pmatrix} \boldsymbol{I} & 0 \\ \frac{\boldsymbol{u}_k(\psi_{ij})^\mathsf{T}}{d_{ij,k}} & \frac{d_{ij,k+1}}{d_{ij,k}} \end{pmatrix} \tag{30} $$
$$ \boldsymbol{b}_k = \begin{pmatrix} \boldsymbol{u}_k(\psi_{ij}) \\ -\frac{\|\boldsymbol{u}_k(\psi_{ij})\|^2 + d_{ij,k+1}^2 - d_{ij,k}^2}{2\, d_{ij,k}} \end{pmatrix} \tag{31} $$

The elements of the matrices $\boldsymbol{Q}$, $\boldsymbol{c}$ and e depend quadratically on $\boldsymbol{T}(\psi_{ij})$. We omit a full presentation of the component-wise heading angle dependent recursion for the sake of space.

D. Decentralized Control

Since the focus of this work lies on relative pose estimation within a swarm formation, a heuristic control method is applied. Each UAV computes a target position displacement $\Delta\boldsymbol{p}_i^*$, supposed to unilaterally decrease the formation error. A static feedback law then yields a target velocity ${}_{L_i}\boldsymbol{v}_{\mathrm{CMD},i}$ from a proportional controller with gain $k_{xy} = 1$ for the horizontal and $k_z = 0.5$ for the vertical components. The norm of the 3D velocity control output is further saturated to $v_{\mathrm{SAT}} = 0.3\,\mathrm{ms}^{-1}$.

The computation of the target position displacement $\Delta\boldsymbol{p}_i^*$ is done in two steps. First, a yaw angle transformation $\boldsymbol{T}_{L_iF}^*$ of the formation is found such that UAV i's estimates of the other UAVs' relative positions best align with the desired formation. In a second step, given $\boldsymbol{T}_{L_iF}^*$, the target position displacement $\Delta\boldsymbol{p}_i^*$ is found as in Equation 32, where $\Delta_{f,ij} = {}_F\boldsymbol{f}_j - {}_F\boldsymbol{f}_i$ and ${}_F\boldsymbol{f}_i$ is the target position of drone i expressed in the formation frame.

$$ \Delta\boldsymbol{p}_i^* = \underset{\Delta\boldsymbol{p}_i}{\arg\min} \frac{1}{2} \sum_{j=1, j\neq i}^{n} \left\| {}_{L_i}\hat{\boldsymbol{d}}_{ij} - \Delta\boldsymbol{p}_i - \boldsymbol{T}_{L_iF}^*\, \Delta_{f,ij} \right\|^2 \tag{32} $$

Applying this control law could cause the whole swarm to drift rapidly. As a countermeasure, we chose to have drone 0 as a leader, which does not apply any control action. Instead,

it hovers over the take-off location, relying on local odometry measurements so that the swarm is "anchored" by the leader.

IV. Experimental Results

The algorithms presented in this paper are practically implemented and evaluated on a swarm of five nano-UAVs – i.e., UAVs that weigh below $50\,\mathrm{g}$ and measure about $10\,\mathrm{cm}$, however, the solution can be adopted for UAVs of every size. Specifically, we use the commercial Crazyflie nano-UAV platform from Bitcraze, which is open source, so the proposed solution can be implemented and evaluated.

A. Experimental Setup and Implementation

Each nano-UAV is equipped with a *FlowDeck v2* that enables velocity measurements and a *Loco positioning deck* that allows to acquire UWB range measurements. We implement a double-sided two-way-ranging [19] that involves two agents (i.e., nano-UAV) at a time and typically requires three UWB messages to obtain the range. Since only one agent gets to compute the range out of the UWB timestamps, we also send an additional fourth data message containing the range to the second agent – so both agents have an estimation of the point-to-point distance. In our ranging scheme, UAV 0 does ranging with UAVs $1-4$, then UAV 1 does ranging with UAVs $2-4$, and so on. After the last ranging (i.e., UAV 3 with UAV 4), the process is restarted from UAV 0.

Asynchronously, each UAV sends the ranges it acquired along with its estimated velocity and heading at a rate of $10\,\mathrm{Hz}$ to the computer in the loop. The UAVs are resource-constrained, and they can not carry the computation onboard. Thus, the computer runs the relative localization and formation control algorithms previously introduced. Furthermore, at a rate of $10\,\mathrm{Hz}$, it sends back the control information to the swarm UAVs so that they move in the desired formation.

To perform a quantitative evaluation of our algorithms, we use a Vicon Vero 2.2 motion capture system (mocap). We specifically selected the Crazyflie platform because it is characterized by miniaturized low-power sensors, which typically provide poorer accuracy than their standard-size counterparts. Proving the effectiveness of our solutions with such a challenging setup demonstrates the functionality also with the more capable UAV platforms.

B. Experimental Results

We evaluate the performance of the relative localization solution proposed in Section III-B and the formation control algorithm proposed in Section III-C. To assess the *relative localization error*, we use the metric given in Equation 33, where ${}_{L_i}\hat{\boldsymbol{d}}_{ij}$ is the estimated relative localization vector. Note that a UAV i measured the relative position of a UAV j in its local gravity-aligned coordinate frame L_i. Since the ground truth is provided by the mocap, we firstly rotate the estimated relative position into the mocap's frame (using $\hat{\boldsymbol{T}}_{ML_i}$) and then compute the difference w.r.t. the ground truth – ${}_M\boldsymbol{p}_i$ is the measured position vector of UAV i.

$$\text{ERROR}({}_{L_i}\hat{\boldsymbol{d}}_{ij}) = \left\| \hat{\boldsymbol{T}}_{ML_i}\, {}_{L_i}\hat{\boldsymbol{d}}_{ij} - \left({}_M\boldsymbol{p}_j - {}_M\boldsymbol{p}_i\right) \right\| \tag{33}$$

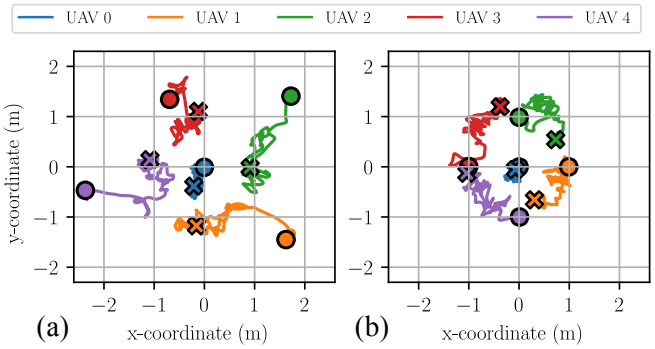

Fig. 3: Ground truth trajectories of the swarm for the two experiments. (a) in the first experiment, the swarm convergence is assessed with offset initial positions. (b) the stability of the swarm under a minimum of observability-aiding motion is assessed in the second experiment. UAV 0 is the leader. Take-off positions are marked with **o** and landing positions with **x**.

In the following, we also provide an evaluation metric for *formation control error*, which assesses the performance of the whole relative estimation and control loop. We define as ${}_F\boldsymbol{f}_i$ the target position in the formation expressed in a gravity-aligned formation frame. We recall that UAV 0 is the leader, so the formation control error is expressed w.r.t. it. We define as ${}_M\bar{\boldsymbol{f}} = {}_M\boldsymbol{p}_0 - \boldsymbol{T}_{MF}\, {}_F\boldsymbol{f}_1$ the offset between the mocap frame and the formation frame for the leader UAV, where $\boldsymbol{T}_{MF}$ is the transformation matrix from the formation frame to the mocap frame. Therefore the formation control error for one UAV i is defined by Equation 34, quantifying how far a UAV is from its target position in the formation.

$$\text{ERROR}({}_M\boldsymbol{p}_i) = \left\| {}_M\boldsymbol{p}_i - \boldsymbol{T}_{MF}\, {}_F\boldsymbol{f}_i - {}_M\bar{\boldsymbol{f}} \right\| \tag{34}$$

In the first experiment, we evaluate the swarm's capability of going into a predefined formation, assessing the system convergence time and the formation errors. Each of the five UAVs starts from a position that is significantly off from the target position (i.e., about $1\,\mathrm{m}$ – $2\,\mathrm{m}$) in the formation and is chosen so that there is no collision with the other UAVs while reaching the final position. The target formation is defined by a square, where each of the UAVs 1 – 4 has to reach a vertex, while UAV 0 is the center of the square, as shown in Figure 3-(a). To have a closer look at the functionality of the relative localization algorithm, we present the time evolution of the relative positions between UAV 1 and the other UAVs. The results are given in Figure 4, showing both the 3D position and the heading. Due to the space limitation, this paper only presents the estimates of UAV 1, but the results are similar for all other UAVs. One can note that all position estimates converge to a steady value after about $25\,\mathrm{s}$. The convergence is slowed down by poor observability in the near-static formation and by the range measurement noise. The relative localization error averaged over the experiment time is in the range $73\,\mathrm{cm}$ – $90\,\mathrm{cm}$ for each of the four UAVs, with a mean of $78\,\mathrm{cm}$. Furthermore, if we exclude the convergence time from the calculation, the mean becomes $55.5\,\mathrm{cm}$. Excluding the convergence phase, the mean heading estimation error has a value of $24°$ –

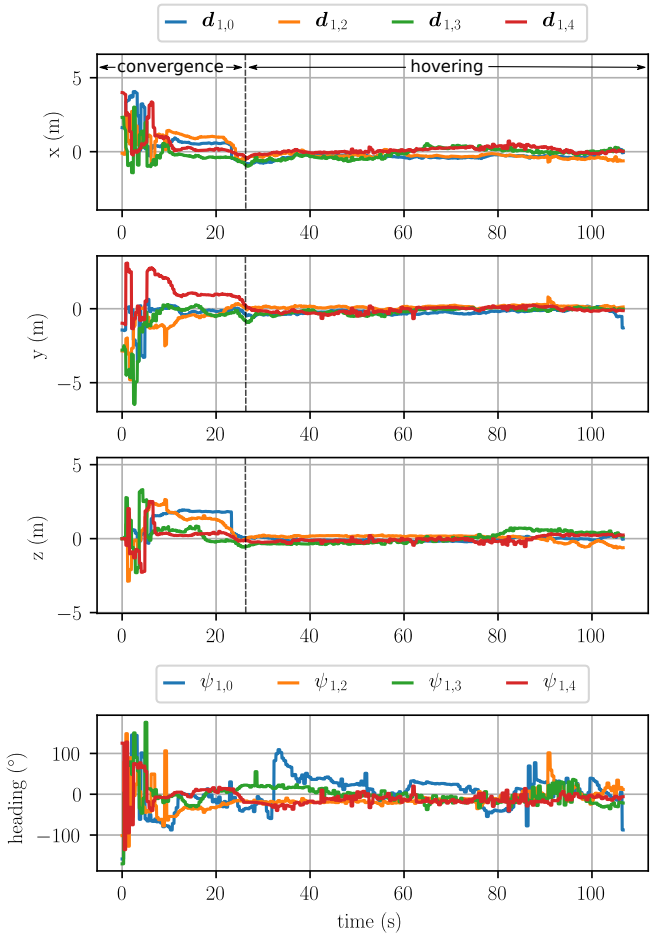

Fig. 4: Relative pose estimation errors for UAV 1 in the first swarm experiment. The convergence time is considered 25 s.

averaged among all nano-UAVs. For 2 – 4, the heading error tends to stay bounded within $\pm 30°$. However, the results are worse for the relative heading of the nano-UAV 0, due to low observability since it is not moving.

In the following, we evaluate the formation control error, which also considers the performance of the formation control algorithm. Figure 5 shows the formation error curves for each UAV. Since UAV 0 is the leader, its formation error is 0 m. Averaging over the experiment time and all non-leader UAVs, the formation control error is 47.5 cm and 38.5 cm for the cases with and without the convergence time.

In the second experiment, the UAVs take off already in perfect formation. Thus, the goal is to assess the swarm's stability without any stimulated motion that could potentially aid the observability of the relative poses. The trajectories of the UAVs are shown in Figure 3-(b). The relative position error averaged over the experiment time (for $\boldsymbol{d}_{1,0} - \boldsymbol{d}_{1,4}$) is in the range 51 cm – 99 cm, with a mean of 61 cm. Furthermore, the mean heading error is 25°, and the mean formation control error is 41.5 cm. Figure 3-(b) shows that although the drones manage to keep the formation throughout the experiment, the formation frame rotates w.r.t. the mocap frame. This happens because the drones are mainly stationary, and therefore their heading angle becomes unobservable.

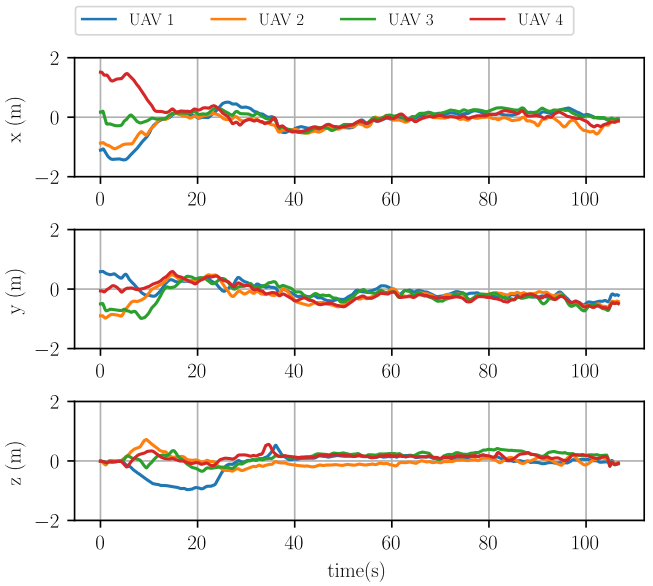

Fig. 5: Formation control errors of the non-leader UAVs in the first experiment. The mean formation error is 47.5 cm.

V. Discussion

A. Error Sources in the Relative Localization

The relative pose estimation takes UWB range measurements and velocity measurements as inputs, which are both affected by non-negligible errors. Integrating the velocity measurement error throughout the performed experiments results in an average of about 50 cm. However, the odometry error is not easy to model as it mainly relies on an optical flow sensor and depends on many factors, such as moving velocity, acceleration, or ground texture [20]. Moreover, only the roll and pitch angles of the odometry frame are observable, while the heading is estimated by relying only on angular velocity integration. Therefore, the heading angle is subject to drift in all our experiments, where it was empirically found to be below 3°. With an assumed upper bound of 3° on the heading drift and an upper bound on the traveled distance of 2 m, the odometry error due to heading drift is bounded by $\sin(3°/2) \cdot 2\,\mathrm{m} \approx 10\,\mathrm{cm}$.

Another error source comes from the UWB range measurements. Due to multi-path, non-line-of-sight conditions, and non-omnidirectional radiation patterns [19], UWB ranging errors are notoriously hard to characterize. In our experiments, we observed an average ranging error of about 10 cm. Among the mentioned sources, odometry errors seem to have the biggest impact on the UAV's positioning accuracy.

B. Comparison with the SoA

The work presented in [5] tackles the relative localization problem using the same sensor information as in this paper. The formation control error obtained in our experiments (i.e., 38.5 cm) is comparable to the one reported in [5], which provides a mean error of 50.8 cm for their leader-follower implementation with two UAVs. However, their EKF-based method requires initial values, and incorrect settings can lead

to robustness issues. The work in [4] employs the same hardware as in our work and extends the methods in [5] by proposing an initialization procedure. They achieve a similar accuracy to our work, but the initialization takes about $30\,\mathrm{s}$, resulting in a total time of $71\,\mathrm{s}$ for going in formation. In contrast, our work requires $25\,\mathrm{s}$ for the same number of drones. The relative localization accuracy depends on the UWB ranging biases, which in [4] are reported to be smaller than $5\,\mathrm{cm}$ due to their distance-based correction. However, the ranging errors also depend on the UWB antennas' relative orientation, and therefore a distance-based only compensation will only be effective for specific orientations [19].

The authors in [5] and [4] apply a leader-follower formation with observability-aiding dynamic trajectory and 2D position estimation, while this paper focuses on a near static formation with 3D position estimation; like our work, both methods estimate the relative heading without absolute heading measurement. In terms of robustness and convergence, in comparison to the EKF-based methods [4], [5], our method does not require initial values. Furthermore, because our method finds a global optimum to the cost function, estimates can quickly recover from wrong values that temporarily misleading sensor data can cause (see Figure 4).

VI. Conclusion

This paper presented a relative pose estimation algorithm that, in conjunction with a swarm control method, enables near-static formation, practically evaluated on a swarm of nano-UAVs with inter-UAV communication and ranging at a rate of $250\,\mathrm{Hz}$. The robustness and accuracy of the proposed approach have been demonstrated with practical experiments, where the nano-UAVs draw the necessary motion for the relative pose estimation solely from control inaccuracies. With a mean formation error of $38.5\,\mathrm{cm}$, the accuracy of our method is comparable to the SoA EKF-based method of Van der Helm et al. [5], while not relying on observability-aiding motion or accurate initial values for the pose estimation. Field results confirmed the ability of the relative pose estimation algorithm to cope with minimal relative motion and noisy measurements. Formulating the relative localization as an optimization problem makes our solution immune to convergence issues observed with EKFs [5], [10], [12].

References

[1] Y. Zhou, B. Rao, and W. Wang, "Uav swarm intelligence: Recent advances and future trends," *IEEE Access*, vol. 8, pp. 183 856–183 878, 2020.

[2] V. Hoang, M. D. Phung, T. H. Dinh, and Q. P. Ha, "Angle-encoded swarm optimization for uav formation path planning," in *2018 RSJ International Conference on Intelligent Robots and Systems (IROS)*. IEEE, 2018, pp. 5239–5244.

[3] M. Coppola, K. N. McGuire, K. Y. W. Scheper, and G. C. H. E. de Croon, "On-board communication-based relative localization for collision avoidance in micro air vehicle teams," *Autonomous Robots*, vol. 42, pp. 1787–1805, 2018. [Online]. Available: https://doi.org/10.1007/s10514-018-9760-3

[4] S. Li, M. Coppola, C. De Wagter, and G. C. de Croon, "An autonomous swarm of micro flying robots with range-based relative localization," *arXiv preprint arXiv:2003.05853*, 2020.

[5] S. van der Helm, M. Coppola, K. McGuire, and G. C. H. E. de Croon, "On-board range-based relative localization for micro air vehicles in indoor leader-follower flight," *Autonomous Robots*, vol. 44, pp. 415–441, mar 2019. [Online]. Available: https://doi.org/10.1007/s10514-019-09843-6

[6] L. Bartolomei, L. Teixeira, and M. Chli, "Semantic-aware active perception for uavs using deep reinforcement learning," in *2021 IEEE/RSJ International Conference on Intelligent Robots and Systems (IROS)*. IEEE, 2021, pp. 3101–3108.

[7] J. P. Queralta, C. M. Almansa, F. Schiano, D. Floreano, and T. Westerlund, "Uwb-based system for uav localization in gnss-denied environments: Characterization and dataset," in *2020 IEEE/RSJ International Conference on Intelligent Robots and Systems (IROS)*. IEEE, 2020, pp. 4521–4528.

[8] V. Niculescu, D. Palossi, M. Magno, and L. Benini, "Fly, wake-up, find: Uav-based energy-efficient localization for distributed sensor nodes," *Sustainable Computing: Informatics and Systems*, vol. 34, p. 100666, 2022.

[9] T. Nägeli, C. Conte, A. Domahidi, M. Morari, and O. Hilliges, "Environment-independent formation flight for micro aerial vehicles," in *2014 IEEE/RSJ International Conference on Intelligent Robots and Systems*, 2014, pp. 1141–1146. [Online]. Available: https://ieeexplore.ieee.org/document/6942701

[10] X. S. Zhou and S. I. Roumeliotis, "Robot-to-robot relative pose estimation from range measurements," *IEEE Transactions on Robotics*, vol. 24, no. 6, pp. 1379–1393, 2008. [Online]. Available: https://ieeexplore.ieee.org/document/4671092

[11] S. Wang, D. Gu, L. Chen, and H. Hu, "Single beacon-based localization with constraints and unknown initial poses," *IEEE Transactions on Industrial Electronics*, vol. 63, no. 4, pp. 2229–2241, 2016. [Online]. Available: https://ieeexplore.ieee.org/document/7323837

[12] K. Guo, Z. Qiu, W. Meng, L. Xie, and R. Teo, "Ultra-wideband based cooperative relative localization algorithm and experiments for multiple unmanned aerial vehicles in gps denied environments," *International Journal of Micro Air Vehicles*, vol. 9, no. 3, pp. 169–186, 2017. [Online]. Available: https://doi.org/10.1177/1756829317695564

[13] S. Güler, M. Abdelkader, and J. S. Shamma, "Peer-to-peer relative localization of aerial robots with ultrawideband sensors," *IEEE Transactions on Control Systems Technology*, vol. 29, no. 5, pp. 1981–1996, 2021. [Online]. Available: https://ieeexplore.ieee.org/document/9217573

[14] W. Navidi, W. S. Murphy, and W. Hereman, "Statistical methods in surveying by trilateration," *Computational Statistics & Data Analysis*, vol. 27, no. 2, pp. 209–227, 1998. [Online]. Available: https://www.sciencedirect.com/science/article/pii/S0167947397000534

[15] M. Larsson, V. Larsson, K. Astrom, and M. Oskarsson, "Optimal trilateration is an eigenvalue problem," in *ICASSP 2019 - 2019 IEEE International Conference on Acoustics, Speech and Signal Processing (ICASSP)*, 2019, pp. 5586–5590. [Online]. Available: https://ieeexplore.ieee.org/document/8683355

[16] G. Vásárhelyi, C. Virágh, G. Somorjai, N. Tarcai, T. Szörenyi, T. Nepusz, and T. Vicsek, "Outdoor flocking and formation flight with autonomous aerial robots," in *2014 IEEE/RSJ International Conference on Intelligent Robots and Systems*, 2014, pp. 3866–3873. [Online]. Available: https://ieeexplore.ieee.org/document/6943105

[17] I. Dotlic, A. Connell, H. Ma, J. Clancy, and M. McLaughlin, "Angle of arrival estimation using decawave dw1000 integrated circuits," in *2017 14th Workshop on Positioning, Navigation and Communications (WPNC)*, 2017, pp. 1–6. [Online]. Available: https://ieeexplore.ieee.org/abstract/document/8250079

[18] A. Ledergerber, M. Hamer, and R. D'Andrea, "Angle of arrival estimation based on channel impulse response measurements," in *2019 IEEE/RSJ International Conference on Intelligent Robots and Systems (IROS)*, 2019, pp. 6686–6692. [Online]. Available: https://ieeexplore.ieee.org/document/8967562

[19] L. Flueratoru, S. Wehrli, M. Magno, E. S. Lohan, and D. Niculescu, "High-accuracy ranging and localization with ultrawideband communications for energy-constrained devices," *IEEE Internet of Things Journal*, vol. 9, no. 10, pp. 7463–7480, 2022. [Online]. Available: https://ieeexplore.ieee.org/document/9600447

[20] R. Siegwart, I. R. Nourbakhsh, and D. Scaramuzza, *Introduction to autonomous mobile robots*. MIT press, 2011.